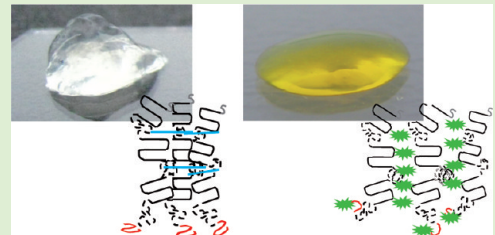


Controlled Hydrogel Formation of a Recombinant Spider Silk Protein

Kristin Schacht and Thomas Scheibel*

Lehrstuhl Biomaterialien, Fakultät Angewandte Naturwissenschaften, Universität Bayreuth, Universitätsstr. 30, 95440 Bayreuth, Germany

ABSTRACT: Due to their biocompatibility, biodegradability, and low immunogenicity, recombinant spider silk proteins have a high potential for a variety of applications when processed into morphologies such as films, capsules, beads, or hydrogels. Here, hydrogels made of the engineered and recombinantly produced spider silk protein eADF4(C16) were analyzed in detail. It has previously been shown that eADF4(C16) nanofibrils self-assemble by a mechanism of nucleation-aggregation, providing the basis of silk hydrogels. We focused on establishing a reproducible gelation process by employing different protein concentrations, chemical crosslinking, and functionalization of eADF4(C16) with fluorescein. Fluorescein strongly influenced assembly as well as the properties of the hydrogels, such as pore sizes and mechanical behavior, possibly due to its interference with packing of silk nanofibrils during hydrogel formation.



INTRODUCTION

In comparison to other arthropods, spiders produce more than one silk type with various functions and properties.¹ Female orb-weaving spiders use up to six different silks and a silk-like glue.^{2,3} Some silk fibers exhibit excellent mechanical properties such as high tensile strength combined with good extensibility.^{1,2} Dragline silk, which forms the frame and radii of orb webs, is the best characterized spider silk.^{1,2,4,5} Dragline silk is mainly composed of two large proteins (spidroins), which, in the case of the garden spider *Araneus diadematus*, are named ADF3 (*A. diadematus* fibroin) and ADF4.⁶ Spidroins generally have a highly repetitive core sequence consisting of several tandem repeats of distinct consensus motifs.^{2,6} Polyalanine motifs A_n or (GA)_n (A: alanine, G: glycine) form tightly packed β -sheet crystallites, while glycine-rich motifs, for example, GPGXX (P: proline, X: often representing glutamine), can fold into various structures, such as 3₁-helices, turns and random coils, all of which form an amorphous region in which the β -sheet crystallites are embedded.⁴ Mechanically, the β -sheet-rich crystallites are important for the strength of dragline silk, whereas the amorphous matrix is responsible for its extensibility.^{7,8} The repetitive protein core is flanked by two nonrepetitive terminal regions which are critical in the storage of the proteins in the gland and in initiating fiber assembly.^{9–14}

Due to the fact that most spiders are cannibals, farming spiders for large-scale production of silk is not feasible. Therefore, recombinant production of spidroins is important for their application as high performance materials.^{6,15–17} Several recombinant spidroins based on the sequences of both dragline spidroins of *A. diadematus* have been recombinantly produced in *E. coli*.^{15,16} It has been shown that such recombinant spidroins can be assembled into various morphologies, such as films, capsules, beads, and hydrogels, depending on the processing conditions.^{5,18–26}

Hydrogels are three-dimensional polymer networks that can absorb water, thereby swelling physically, or are solids that have a

water content over 95%.^{20,27,28} Hydrogels for biomedical applications have been made of a variety of naturally and synthetically derived polymers such as agarose, alginate, chitosan, collagen, poly(acrylic acid) (PAA), poly(vinyl alcohol) (PVA), and poly(ethylene oxide) (PEO).²⁹ The hydrogel structure can be formed by the connectivity of the polymer chains through either physical or chemical crosslinking. With self-assembling systems it is also possible to form hydrogels from nonbranched fibers, where the hydrogel forms due to the density of fibers, preventing the movement of water and fibers.

The biocompatibility, biodegradability, and low immunogenicity of silk proteins make them ideal for applications such as scaffolds for tissue engineering and drug delivery but also for technical applications such as a space filling agent or functional coating.^{20,27–30} The recombinant, engineered spider silk protein eADF4(C16) consists of 16 repeats of a module named C (sequence: GSSAAAAAAAASGPGGY PENQGPGSGPGGY-GPGGP) mimicking the repetitive part of the dragline silk fibroin ADF4 of the garden cross spider (*Araneus diadematus*). eADF4-(C16) has been previously shown to self-assemble into stable hydrogels under defined conditions.²⁰ Silk nanofibrils self-assemble through a mechanism of nucleation-aggregation followed by a concentration-dependent gelation.^{20,25,30,31} During gelation, the protein chains arrange into physically crosslinked β -sheet structures by hydrophobic interactions and entanglements.^{31–33} Due to their semiflexible nature, spider silk hydrogels have viscoelastic properties and comprise structures similar to that of other networks of biopolymers.^{20,33}

Here, a reproducible processing route for the formation of hydrogels of eADF4(C16) is established. The resulting hydrogels are characterized concerning their morphology, structure,

Received: February 1, 2011

Revised: May 11, 2011

Published: May 26, 2011

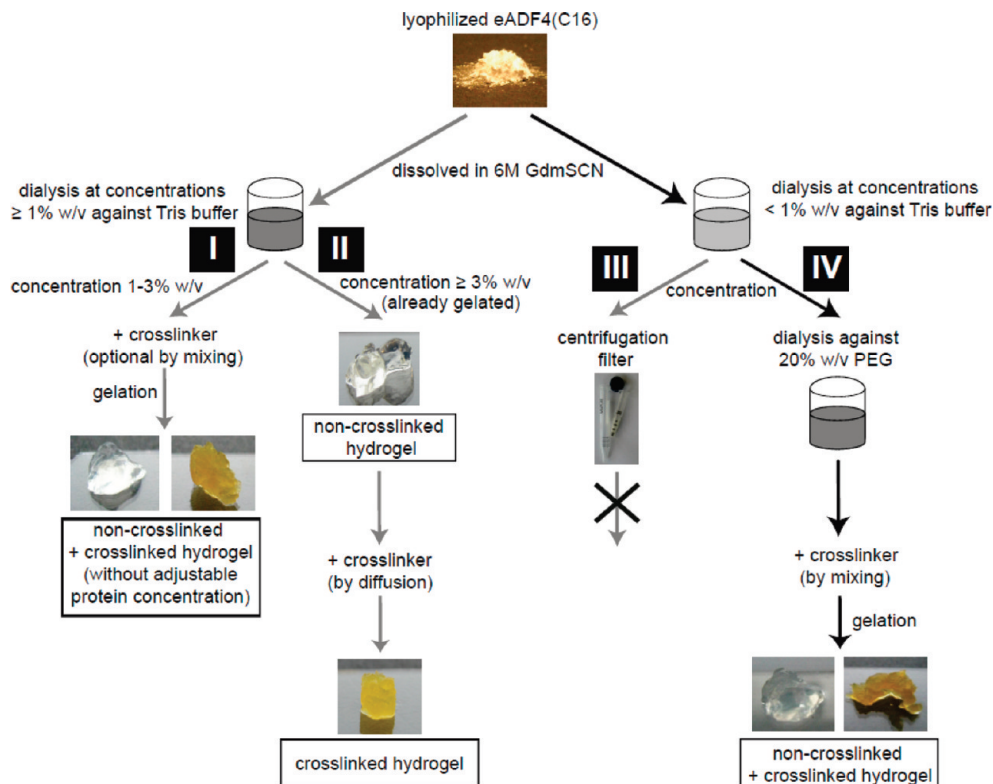


Figure 1. Four tested routes of hydrogel formation.

and rheology. To further control the eADF4(C16) hydrogel's properties, chemical crosslinking and functionalization with fluorescein were accomplished. The results provide mechanistic insights into eADF4(C16) hydrogel assembly, which will allow further investigation into its potential for distinct applications.

■ EXPERIMENTAL SECTION

Production of eADF4(C16). The engineered protein eADF4(C16) consists of 16 repeats of a module named C (sequence: GSSAAAAAAASGPGGYGPENQGPGSGPGGYGPGGP) mimicking the repeated sequence motif of the dragline silk protein ADF4 of the garden cross spider (*Araneus diadematus*).¹⁵ eADF4(C16) was produced and purified as described previously.¹⁵

Hydrogel Formation by Dialysis. Lyophilized eADF4(C16) was dissolved in 6 M guanidinium thiocyanate at concentrations ranging from 30 mg/mL (3% w/v) to 70 mg/mL (7% w/v) and dialyzed using dialysis membranes with a molecular weight cutoff of 6000–8000 Da against 10 mM Tris/HCl, pH 7.5, overnight at room temperature. All hydrogels were stored for at least 4 days at 4 °C before analysis. The final protein concentrations were determined photometrically at 280 nm after denaturation of the hydrogels in 8 M guanidinium hydrochloride.

Hydrogel Formation by Water Removal (PEG Dialysis). No hydrogels formed during dialysis of eADF4(C16) solutions at concentrations between 3 and 7 mg/mL against Tris/HCl, pH 7.5, at room temperature. Solutions at concentrations between 10 and 30 mg/mL started gelling uncontrollably after dialysis. Solutions at concentrations below 10 mg/mL were stable under our experimental conditions. Subsequent dialysis of the later solutions against 20% w/v PEG (20,000 g/mol) at a volume ratio of PEG to eADF4(C16) solution of 100:1 removed water by osmotic stress and allowed a defined adjustment of protein concentration.^{31,35} This technology has been reproduced by four independent researchers in our laboratory.

Crosslinking of eADF4(C16) Hydrogels. Hydrogels were gently mixed with a 20-fold molar excess of ammonium peroxodisulfate (APS; Roth, Germany) and 100:1 tris(2,2'-bipyridyl)dichlororuthenium(II) (Rubpy; Sigma-Aldrich, Germany) after dialysis to avoid shear-induced artifacts. After 2 days of incubation in the dark at 4 °C, the hydrogels were exposed to visible light from a tungsten lamp for 2 min to initiate crosslinking.³⁶

Analysis of Swelling Behavior of eADF4(c16) Hydrogels. eADF4(C16) Hydrogels (3, 5, and 7%, crosslinked and non-crosslinked) were analyzed concerning their volume prior to drying. Drying was accomplished by incubation at 60 °C for 4 days. The decrease in volume upon drying was between 6- and 15-fold. After drying, the samples were incubated in an excess volume of 10 mM Tris/HCl, pH 7.5, for 24 h. While non-crosslinked samples started to swell and to disassociate into suspended nanofibrils (which also happened upon increasing the buffer volume of freshly made non-crosslinked hydrogels), crosslinked hydrogels swelled between 5 to 10-fold, but remained stable without any apparent disassociation.

Coupling of Fluorescein and eADF4(C16). Lyophilized eADF4(C16) was dissolved in 6 M guanidinium thiocyanate (GdmSCN) and dialyzed against 10 mM HEPES, pH 8.0. Dialyzed eADF4(C16) was incubated with a 15-fold molar excess of (S(6)-carboxyfluorescein-N-hydroxysuccinimide ester (Sigma-Aldrich, USA) in the dark for 2.5 h at room temperature. After incubation, proteins were precipitated by addition of 2 M potassium phosphate, pH 7.0, for 30 min. Precipitated proteins were washed three times with water followed by lyophilization.

Analysis of Gelation Kinetics. A total of 200 µL of eADF4(C16) solution (30 mg/mL in Tris/HCl, pH 7.5) per well were placed in covered 96-well plates (Roth, Germany) after dialysis against Tris buffer. Turbidity changes upon gelation were monitored at 570 nm using a Microplate Reader (Mithras LB 940, Berthold Technologies, Germany) in absorbance mode. Each experiment was performed three times and the shown graphs represent mean values ± s.d.

Scanning Electron Microscopy (SEM). SEM was performed using a XL 30 ESEM (Philips) with a high tension voltage of 15 kV. To analyze their morphological structure, eADF4(C16) hydrogels were chemically fixed with a fixation buffer (2.5% v/v glutaraldehyde, 80 mM HEPES, 3 mM CaCl₂, pH 7.3) at room temperature, followed by incubation for 3 h at 4 °C. Then, samples were washed with water four times, frozen at -80 °C, and lyophilized. The lyophilized samples were then sputtered with gold by vacuum evaporation for 2 min.

Fourier-Transform Infrared Spectroscopy (FTIR). Infrared spectroscopy was conducted in absorbance mode using a Bruker Tensor 27 spectrometer (Bruker, Germany). Lyophilized samples were placed on an ATR-crystal and pressed with a stamp. Each measurement comprised a 60-scan interferogram with a 2 cm⁻¹ resolution between 3500 and 800 cm⁻¹. The amide I region (1590–1720 cm⁻¹) was analyzed by Fourier self-deconvolution (FSD) using OPUS software (version 6.5). Bands were assigned to secondary structure elements according to Hu et al., 2006.³⁷ The presented secondary structure contents reflect the mean values ± s.d. derived from three independent samples, which were deconvoluted three times each.

Rheological Properties. Rheological measurements of eADF4(C16) hydrogels were performed using a Physica MCR 500 with 25 mm parallel plate–plate geometry (PP 25). Stress–strain curves were determined at 25 °C. After loading the sample (1 mL), the upper plate was slowly lowered until the desired gap of 1 mm was reached. Afterward, the excess solution was gently soaked off. A solvent trap with a wet sponge was used to minimize evaporation. Shear (G) and elastic (E) moduli were calculated according to Hooke's law using the Possion's ratios published by Urayama et al., 1993, and Johnson et al., 2004.^{38–40}

RESULTS AND DISCUSSION

A reproducible gelation process is important when hydrogels are employed as a material, for example, in tissue engineering. Therefore, different routes of hydrogel formation were analyzed in parallel to determine the most reproducible one (Figure 1). The recombinant spider silk protein eADF4(C16) was denatured in 6 M GdmSCN and subsequently dialyzed against 10 mM Tris/HCl, pH 7.5. It has previously been shown that eADF4(C16) spontaneously self-assembles into hydrogels,^{22,41} however, here control over this gelation process was desired by variation of the processing conditions.

eADF4(C16) Hydrogel Formation in Dependence of Protein Concentration. During dialysis against Tris/HCl, eADF4(C16) with concentrations between 10 and 30 mg/mL did not cause gelling inside the dialysis tube, but shortly after removal of the solution (Figure 1, route I). Because no precise protein concentration could be adjusted, further handling was complicated. During dialysis, higher concentrated eADF4(C16) solutions (above 30 mg/mL) even spontaneously self-assembled into hydrogels inside the dialysis membrane (route II). Lower concentration solutions (3–7 mg/mL) showed no gelation during or after dialysis. To initiate hydrogel formation in a controlled manner therein, the protein concentration had to be increased in a controllable manner. Two different concentrating techniques were tested: centrifugation through a filter (route III) and dialysis against 20% w/v PEG (route IV). During centrifugation, gelation occurred on top of the filter, again complicating further handling. However, route IV (Figure 1) allowed the reproducible adjustment of protein concentration after removing the solution from the dialysis tube before hydrogel formation started.

The derived hydrogels showed a low stability, because upon addition of an excess volume of buffer (after hydrogel formation

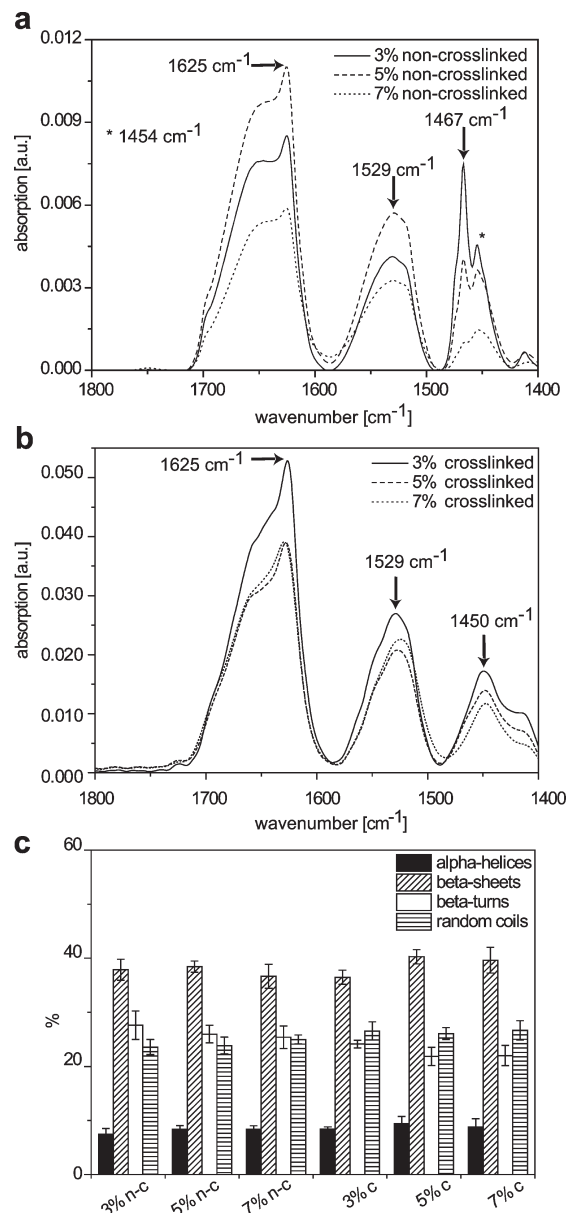


Figure 2. Fourier-transform infrared spectra of non-crosslinked (a) and crosslinked (b) eADF4(C16) hydrogels at different protein concentrations. (c) Secondary structure distribution in eADF4(C16) hydrogels as mean values ± s.d. derived from three independent samples, which were deconvoluted three times each using Fourier self-deconvolution (FSD) of the amide I band; n-c, non-crosslinked; c, crosslinked.

was finished), the hydrogels slowly disassembled over days, sparing suspended eADF4(C16) nanofibrils.

Chemical Crosslinking of eADF4(C16) Hydrogels. To stabilize the three-dimensional structure of the hydrogels, chemical crosslinking was used to connect the tyrosine residue side chains of eADF4(C16) (which contains 32 tyrosines) using ammonium peroxodisulfate (APS) and tris(2,2'-bipyridyl)dichlororuthenium(II) (Rubpy), as previously described.^{22,36} At low protein concentrations, the cross-linker was applied by gently mixing after dialysis (route I). Alternatively, the cross-linker was incubated with hydrogels, and diffusion was used to incorporate the cross-linker throughout the hydrogel (route II). The most

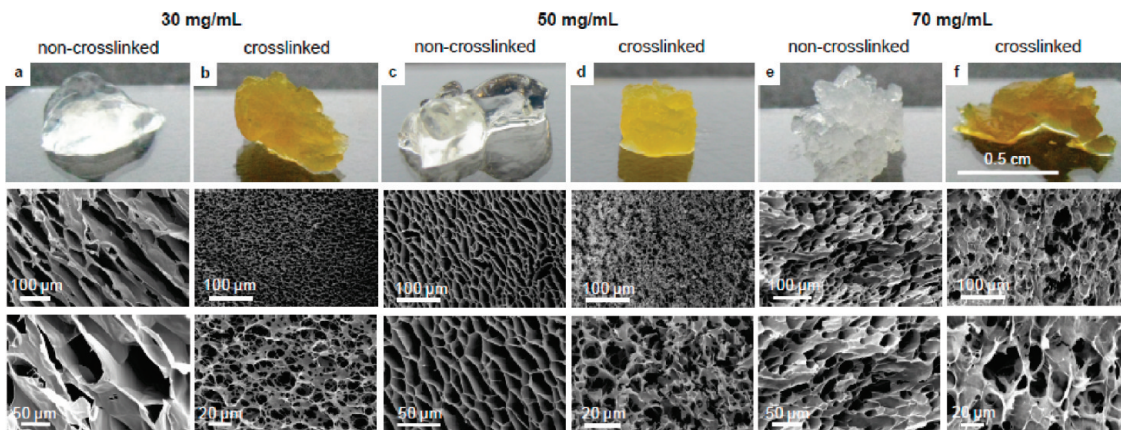


Figure 3. Macroscopic and SEM images of non-crosslinked (a, c, e) and crosslinked (b, d, f) eADF4(C16) hydrogels at different concentrations (30, 50, and 70 mg/mL). All macroscopic samples have an identical scale.

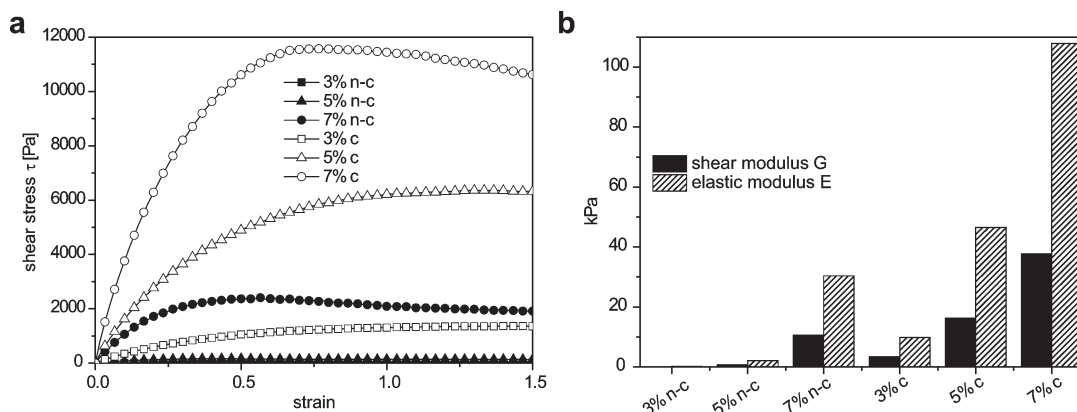


Figure 4. Rheological measurements (stress–strain curves) of non-crosslinked and crosslinked eADF4(C16) hydrogels at 25 °C. Due to large sample sizes necessary for the measurement, each hydrogel class was measured in single experiments. (a) Stress–strain curves of eADF4(C16) hydrogels at different protein concentrations; (b) Shear moduli (G) and elastic moduli (E) of eADF4(C16) hydrogels; n-c, non-crosslinked; c, crosslinked.

reproducible results were obtained by adding the cross-linker to eADF4(C16) solutions after dialysis against PEG. As mentioned above, route IV (Figure 1) provided the highest processing reproducibility and was therefore used for all further experiments.

The gained hydrogels were stable in an excess of buffer. To analyze the swelling behavior, hydrogels were slowly dried and then rehydrated with 10 mM Tris/HCl, pH 7.5. The increase in volume between the dried and the swollen state was on average between 5- and 10-fold in all hydrogels without any apparent disassociation.

Structural Analysis of Hydrogels. The gelation process of eADF4(C16) is accompanied by the transition of α -helical and random coil conformations in solution into β -sheet-rich ones in nanofibrils. Both the influence of varying protein concentrations as well as the impact of chemical crosslinking on the secondary structure were analyzed by FTIR spectroscopy (Figure 2a,b). The IR-absorbance maxima at 1625 and 1529 cm^{-1} are characteristics of β -sheet-rich conformations. Regardless of the protein concentration, all hydrogels showed an overall β -sheet content between 37 and 41% (Figure 2c) without a clear influence of protein concentration or crosslinking, as analyzed by Fourier self-deconvolution (FSD). Minor differences in β -sheet structure between non-crosslinked and crosslinked hydrogels and between hydrogels made at different protein concentrations were

observed in the spectral region between 1470 and 1450 cm^{-1} . All hydrogels showed a maxima at 963 cm^{-1} , indicating that the polyalanine regions of eADF4(C16) were in a β -sheet conformation (data not shown).^{42,43} Taken together, these findings indicated that nanofibrils in all samples showed similar secondary structures.

Morphology of Hydrogels. With increasing eADF(C16) protein concentrations, the pore sizes of the hydrogels decreased from around 200 μm (30 mg/mL) to 30 μm (70 mg/mL; Figure 3). After chemical crosslinking, the pore sizes were around 10–20 μm , but this was apparently independent of the protein concentration. While non-crosslinked hydrogels revealed sheet-like morphologies, crosslinked hydrogels resembled a highly interconnected sponge-like material. The morphology change between non-crosslinked and crosslinked hydrogels could be caused by the fact that in non-crosslinked hydrogels smaller pores could fuse during the process of fixation,⁴⁴ which is inhibited by chemical crosslinking prior to fixation.

Rheological Properties of eADF4(C16) Hydrogels. The stiffness of non-crosslinked and crosslinked hydrogels was determined rheologically with plate–plate geometry at 25 °C. eADF4(C16) hydrogels demonstrated viscoelastic properties similar to most concentrated polymer networks.³⁴ The application of a linearly increasing strain caused stress changes proportionally

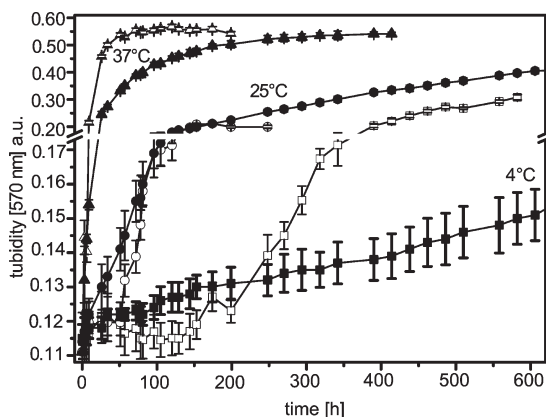


Figure 5. Temperature-dependent turbidity changes (indicative of nanofibril formation) of fluorescein-labeled (filled symbols) and -unlabeled (open symbols) eADF4(C16) hydrogels (30 mg/mL) at temperatures indicated. Changes in turbidity were monitored at 570 nm. Each data point is averaged from three independent samples and s.d. is provided.

to the applied strain. The shear stress was dependent on the protein concentration and on crosslinking (Figure 4a). The shear moduli (G) and elastic moduli (E) increased with increasing protein concentrations (Figure 4b). It is likely that high protein concentrations and chemical crosslinking decrease the mobility of the nanofibrils, inducing an increase in mechanical stiffness.⁴⁵ The elastic moduli of the hydrogels were between 0.2 and 110 kPa, which is in the regime of most human tissues and organs with the exception of bone.²⁶

Effect of Temperature on eADF4(C16) Hydrogel Formation. The influence of temperature on eADF4(C16) hydrogel formation was analyzed by the turbidity of each sample, which was monitored at 570 nm in a time-dependent manner (Figure 5). At 37 °C, the gelation process started immediately and was completed after 80 h. Hydrogel formation started after a short lag-phase and took much longer at 25 °C, while at 4 °C the hydrogel formation started after an extended lag-phase of ~6 days and showed the slowest kinetics. Because it has been shown that eADF4(C16) nanofibrils assemble through a mechanism of nucleation–aggregation, increased temperature permits higher protein mobility, leading to increased nucleus and nanofibril formation. Because higher temperatures further promote hydrophobic interactions,^{41,46,47} nanofibril nucleation and assembly and hydrogel formation would be expected to be highly accelerated as observed here.

Functionalization of eADF4(C16) and Its Influence on Hydrogel Formation. The influence of modifications on the formation of hydrogels by eADF4(C16) was analyzed by functionalization with a fluorescent molecule. As an easily detectable example, 5(6)-carboxyfluorescein-N-hydroxysuccinimide ester was coupled to the amino-terminus of eADF4(C16) at 15-fold molar excess, yielding a coupling efficiency of 2–6 mol fluorescein per mol eADF4(C16). This indicated that nonspecific coupling occurred possibly to hydroxyl groups of tyrosine residues in addition to the intended amino-terminal site. For specific applications, site-specific functionalization is crucial; however, in this case, the lower specificity of coupling was considered to be less of an issue, because analyzing the general influence of additional hydrophobic groups on hydrogel formation of eADF4(C16) was the aim of the study.

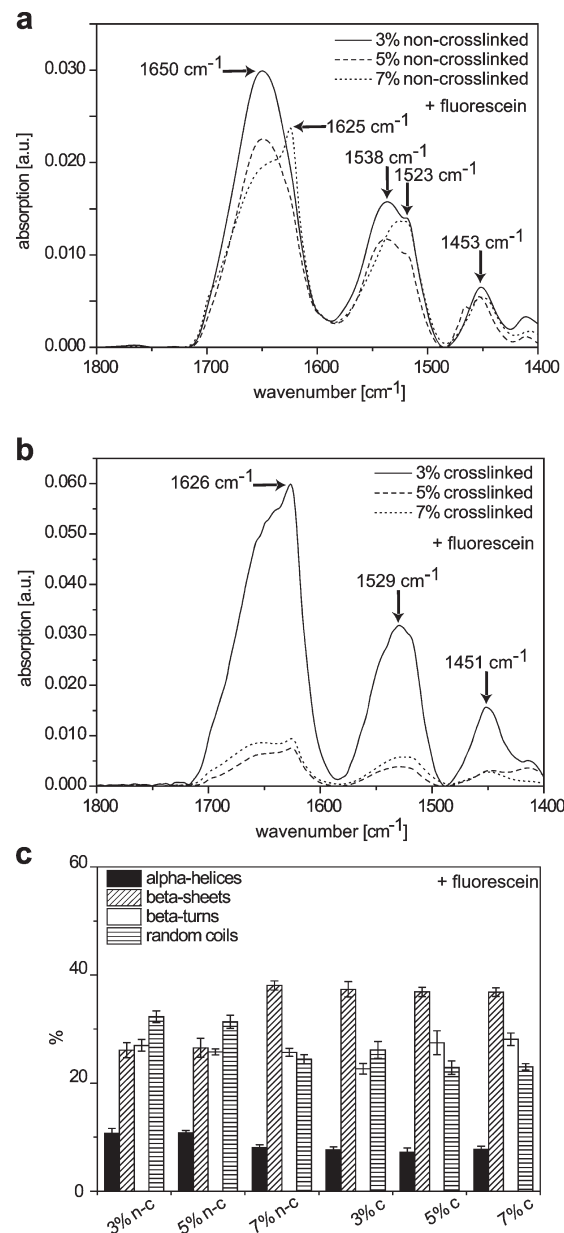


Figure 6. Fourier-transform infrared spectra of non-crosslinked (a) and crosslinked (b) fluorescein-eADF4(C16) hydrogels at different protein concentrations. (c) Secondary structure distribution in fluorescein-eADF4(C16) hydrogels as mean values \pm s.d. derived from three independent samples, which were deconvoluted three times each using Fourier self-deconvolution (FSD) of the amide I band; n-c, non-crosslinked; c, crosslinked.

First, the influence of the presence of coupled fluorescein on eADF4(C16) gelation kinetics was analyzed in relation to the temperature of hydrogel formation. Interestingly, independent of the applied temperature no lag-phase could be observed in the turbidity assay. However, in comparison to unlabeled eADF4(C16), all kinetics of fluorescein-eADF4(C16) were significantly slower at the respective temperatures, indicating an influence of fluorescein on nanofibril and hydrogel formation (Figure 5). The absence of lag-phases was either due to hydrophobic interactions of the labels accelerating nucleation or causing unspecific protein aggregation not yielding nanofibrils and hydrogels (see also below).

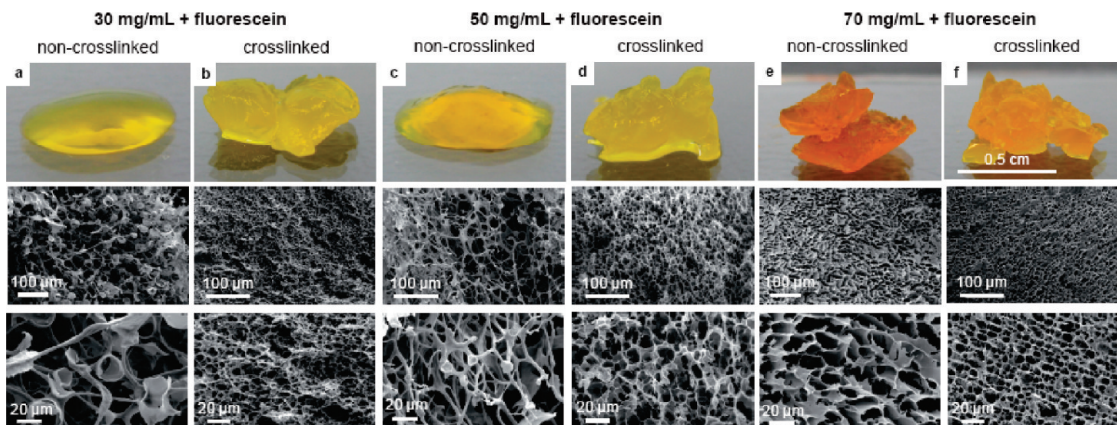


Figure 7. Macroscopic and SEM images of non-crosslinked (a, c, e) and crosslinked (b, d, f) hydrogels of fluorescein-eADF4(C16) at different concentrations (30, 50, and 70 mg/mL). All macroscopic samples have an identical scale.

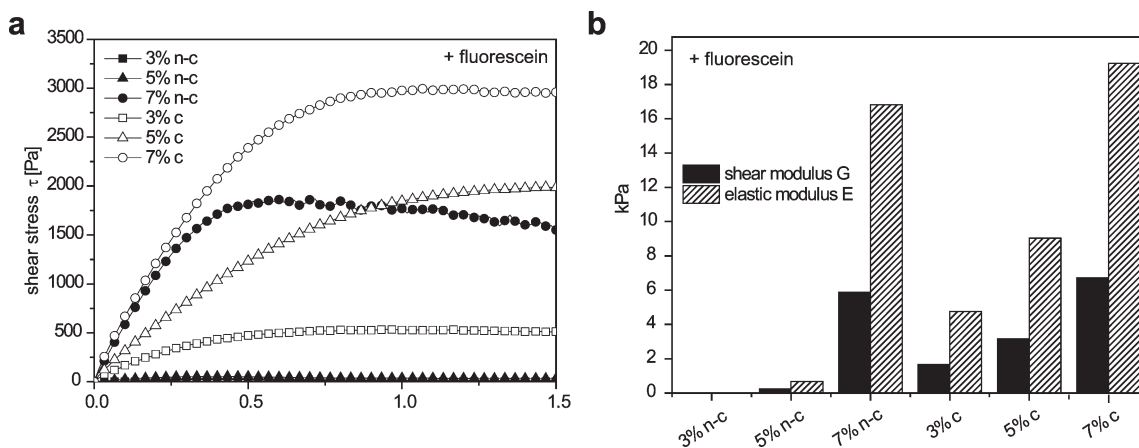


Figure 8. Rheological Measurements (stress–strain curves) of non-crosslinked and crosslinked fluorescein-eADF4(C16) hydrogels at 25 °C. Due to large sample sizes, each hydrogel class was measured in single experiments. (a) Stress–strain curves of fluorescein-eADF4(C16) hydrogels at different protein concentrations; (b) Shear moduli (G) and elastic moduli (E) of eADF4(C16) hydrogels; n-c, non-crosslinked; c, crosslinked.

Structural Analysis of Hydrogels Made of Fluorescein-eADF4(C16). FTIR spectra of non-crosslinked fluorescein-eADF4(C16) hydrogels made at 70 mg/mL revealed IR-absorbance maxima at 1625 and 1523 cm⁻¹ like in non-crosslinked eADF4(C16) hydrogels (Figure 6a). Also, all peak maxima of the amide I and II regions of crosslinked fluorescein-eADF4(C16) hydrogels were at identical wavenumbers in comparison to that of crosslinked hydrogels of unlabeled eADF4(C16) (Figure 6b). These findings were also confirmed by FSD, indicating identical structural content in these hydrogels (Figure 6c). Interestingly, non-crosslinked hydrogels made at concentrations of 30 and 50 mg/mL of fluorescein-eADF4-(C16) revealed spectra with higher content of α -helical and random coil structures, with amide I and II peaks significantly shifted from 1625 to 1650 cm⁻¹ and from 1525 to 1538 cm⁻¹, respectively (Figure 6a). The amount of α -helices (10–12%) and random coil structures (~32%) was calculated by FSD analysis (Figure 6c). This finding was probably due to the fact that nanofibril formation was incomplete (as detected by SEM analysis, see below). Importantly, in all fluorescein-eADF4-(C16) hydrogels the polyalanine regions were in β -sheet conformation identical to polyalanine regions of hydrogels of unlabeled eADF4(C16) (data not shown).

Morphology of Hydrogels Made of Fluorescein-eADF4-(C16). The hydrogels made of fluorescein-eADF4(C16) were not as viscous and compact as those of unlabeled eADF4(C16), although the crosslinked hydrogels looked similar (Figure 7). Hydrogels made of fluorescein-eADF4(C16) had pore sizes that decreased with increasing protein concentration in a similar way to hydrogels of eADF4(C16). Non-crosslinked fluorescein eADF4(C16) hydrogels made of 30 and 50 mg/mL did not have sheet-like morphologies as found in non-crosslinked eADF4(C16) hydrogels but, instead, a network with burst bubbles at the end of the fibrils. This may explain the aberrant secondary structure content.

Rheological Properties of Hydrogels Made of Fluorescein-eADF4(C16). The non-crosslinked fluorescein-eADF4(C16) hydrogels at 30 and 50 mg/mL not only had an aberrant secondary structure content in comparison to all other hydrogels, but also showed properties of viscous liquids rather than hydrogels (Figure 8). All hydrogels (non-crosslinked and crosslinked) made of fluorescein-eADF4(C16) showed a lower strain at linear shear stress in comparison to hydrogels of unlabeled eADF4-(C16), and the elastic moduli were significantly decreased in the labeled counterparts from 35 kPa (70 mg/mL, unlabeled) to 7 kPa (70 mg/mL, labeled). Strikingly, although crosslinked

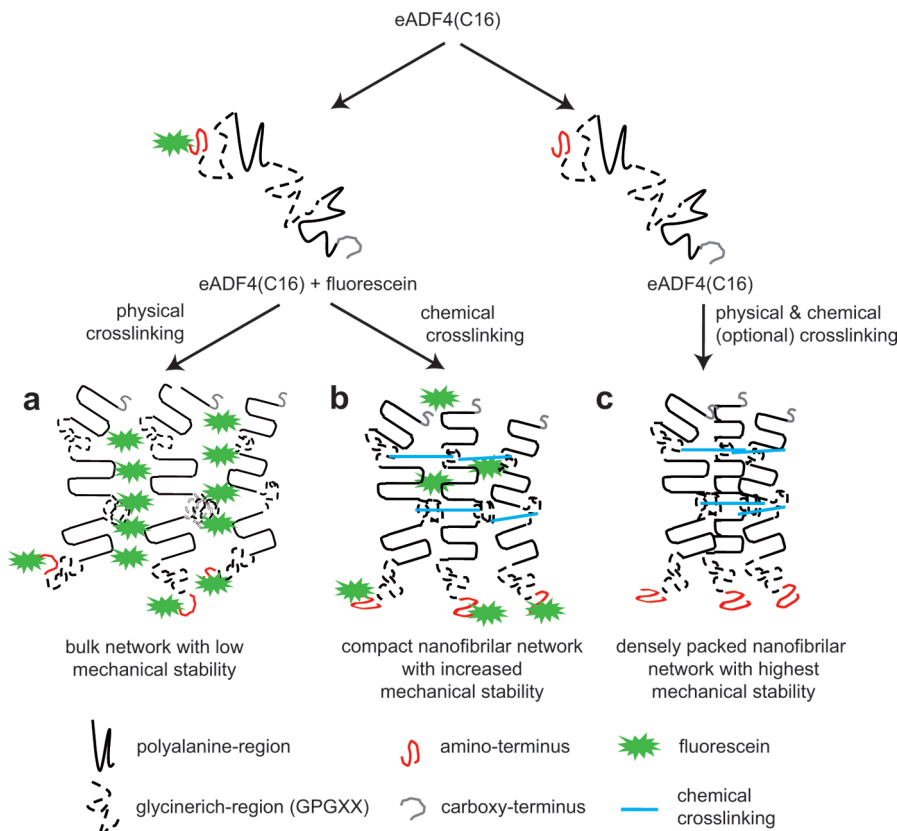


Figure 9. Putative mechanism of eADF4(C16) hydrogel formation. (a) Fluorescein interferes with packing of silk nanofibrils. (b) The hydrogel network is stabilized by chemical crosslinking which competes with the effect of fluorescein on nanofibril/hydrogel packing. Importantly, nonspecific fluorescein coupling to tyrosine residues could also influence (i.e., lower) the crosslinking efficiency of the employed chemical cross-linker. (c) In the absence of fluorescein, eADF4(C16) hydrogels reflect a mechanically stable, densely packed nanofibrillar network (in the presence of a chemical crosslinker mechanical stability is further enhanced).

hydrogels made of fluorescein-eADF4(C16) showed similar secondary structures in comparison to those of unlabeled proteins, the elastic moduli were significantly decreased from about 109 kPa (70 mg/mL unlabeled) to 19 kPa (70 mg/mL labeled; Figure 8).

CONCLUSION

The most reproducible method for hydrogel formation of eADF4(C16) was dialysis of low concentration protein solutions out of 6 M GdmSCN into 10 mM Tris/HCl, pH 7.5, followed by dialysis against a PEG solution. This procedure allowed a controlled increase in protein concentration as well as time to remove the protein solution from dialysis prior to hydrogel formation, simplifying the handling of the silk solution and allowing a controlled hydrogel formation.

With increasing protein concentration, the formation of β -sheet-rich nanofibrils of eADF4(C16) is accompanied by gelation (Figure 9c).²⁸ The morphology and pore size of eADF4(C16) hydrogels depends on the protein concentration and can be influenced by functionalization of the protein and by chemical crosslinking. In crosslinked hydrogels highly interconnected sponge-like networks are formed instead of sheet-like structures which lead to different mechanical properties. In general, the shear and elastic moduli were found to increase with increasing protein concentrations. Chemical crosslinking further stabilized the three-dimensional structure of the eADF4(C16) hydrogels

leading to an additional increase in mechanical strength. The control of pore sizes and mechanical properties is one prerequisite to employ these silk hydrogels for distinct applications.⁴⁸

Functionalization of eADF4(C16) with the hydrophobic molecule fluorescein resulted in a further influence on the mechanical properties of the hydrogels. Fluorescein can potentially interfere with the molecular packing of the nanofibrils inhibiting their stable and regular assembly as seen by the slower assembly kinetics (Figure 9a). This process can partly be outcompeted with chemical crosslinking (Figure 9b). The fact that fluorescein interfered with packing of the nanofibrils can be further seen in the rheological measurements, in which hydrogels of fluorescein-eADF4(C16) showed four to five times lower shear and elastic moduli than hydrogels of unlabeled eADF4(C16). Additionally, due to nonspecific coupling of fluorescein to eADF4(C16), which most likely occurs at tyrosine residues, the amount of cross-linkable tyrosine residues within the hydrogels would be decreased reducing the crosslinking efficiency. This lower degree of chemical crosslinking would further contribute to the lower mechanical strength of crosslinked hydrogels of fluorescein-eADF4(C16).

Thus, by introducing groups that can interfere with the self-assembly of eADF4(C16), it is possible to alter the physical properties of the hydrogels formed by this protein. Additionally, these groups can be used to control the efficiency of chemical crosslinking and control by how much this process increases the rheological properties of the hydrogel. In this way, it may be

possible to tailor hydrogels to be used for example as a scaffold for specific cell types requiring specific mechanical properties.

Taken together, a reproducible process of silk hydrogel formation has been established. The range of adjustable pore sizes from 10 to 200 μm and the range of mechanical strength from 0.1 to 110 kPa provide the basis for testing a variety of applications of spider silk hydrogels.

■ AUTHOR INFORMATION

Corresponding Author

*Phone: +49 (0) 921 55 7361. Fax: +49 (0) 921 55 7346.
E-mail: thomas.scheibel@bm.uni-bayreuth.de.

■ ACKNOWLEDGMENT

We gratefully acknowledge financial support of the DFG (SCHE 603/9-1). We would like to thank Aldo Leal, Carolin Mauerer, and Stefanie Wohlrb for experimental help and Lukas Eisoldt, Andrew Smith, Michael Suhre, and Stefanie Wohlrb for critical comments on the manuscript.

■ REFERENCES

- (1) Vollrath, F. *J. Biotechnol.* **2000**, *74*, 67–83.
- (2) Heim, M.; Keerl, D.; Scheibel, T. *Angew. Chem., Int. Ed.* **2009**, *48*, 3584–3596.
- (3) Romer, L.; Scheibel, T. *Prion* **2008**, *2*, 154–161.
- (4) Heim, M.; Romer, L.; Scheibel, T. *Chem. Soc. Rev.* **2010**, *39*, 156–164.
- (5) Hardy, J.; Scheibel, T. *Prog. Polym. Sci.* **2010**, *35*, 1093–1115.
- (6) Vendrely, C.; Scheibel, T. *Macromol. Biosci.* **2007**, *7*, 401–409.
- (7) Gosline, J. M.; Guerette, P. A.; Ortlepp, C. S.; Savage, K. N. *J. Exp. Biol.* **1999**, *202*, 3295–3303.
- (8) Hayashi, C. Y.; Shipley, N. H.; Lewis, R. V. *Int. J. Biol. Macromol.* **1999**, *24*, 271–275.
- (9) Hagn, F.; Eisoldt, L.; Hardy, J.; Vendrely, C.; Coles, M.; Scheibel, T.; Kessler, H. *Nature* **2010**, *465*, 239–242.
- (10) Askarieh, G.; Hedhammar, M.; Nordling, K.; Saenz, A.; Casals, C.; Rising, A.; Johansson, J.; Knight, S. D. *Nature* **2010**, *465*, 236–238.
- (11) Hagn, F.; Thamm, C.; Scheibel, T.; Kessler, H. *Angew. Chem., Int. Ed.* **2011**, *50*, 310–313.
- (12) Rammensee, S.; Slotta, U.; Scheibel, T.; Bausch, A. *Proc. Natl. Acad. Sci. U.S.A.* **2008**, *105*, 6590–6595.
- (13) Eisoldt, L.; Hardy, J.; Heim, M.; Scheibel, T. *J. Struct. Biol.* **2010**, *170*, 413–419.
- (14) Eisoldt, L.; Smith, A.; Scheibel, T. *Mater. Today* **2011**, *14*, 80–86.
- (15) Huemmerich, D.; Helsen, C. W.; Quedzuweit, S.; Oschmann, J.; Rudolph, R.; Scheibel, T. *Biochemistry* **2004**, *43*, 13604–13612.
- (16) Huemmerich, D.; Scheibel, T.; Vollrath, F.; Cohen, S.; Gat, U.; Ittah, S. *Curr. Biol.* **2004**, *14*, 2070–2074.
- (17) Winkler, S.; Kaplan, D. L. *J. Biotechnol.* **2000**, *74*, 85–93.
- (18) Spiess, K.; Lammel, A.; Scheibel, T. *Macromol. Biosci.* **2010**, *10*, 998–1007.
- (19) Hardy, J. G.; Scheibel, T. *R. Polymer* **2008**, *49*, 4309–4327.
- (20) Rammensee, S.; Huemmerich, D.; Hermanson, K. D.; Scheibel, T.; Bausch, A. R. *Appl. Phys. A: Mater. Sci. Process.* **2006**, *82*, 261–264.
- (21) Slotta, U.; Tammer, M.; Kremer, F.; Koelsch, P.; Scheibel, T. *Supramol. Chem.* **2006**, *18*, 465–471.
- (22) Huemmerich, D.; Slotta, U.; Scheibel, T. *Appl. Phys. A: Mater. Sci. Process.* **2006**, *82*, 219–222.
- (23) Lammel, A.; Schwab, M.; Slotta, U.; Winter, G.; Scheibel, T. *ChemSusChem* **2008**, *5*, 413–416.
- (24) Hermanson, K.; Huemmerich, D.; Scheibel, T.; Bausch, A. *Adv. Mater.* **2007**, *19*, 1810–1815.
- (25) Slotta, U. K.; Rammensee, S.; Gorb, S.; Scheibel, T. *Angew. Chem., Int. Ed.* **2008**, *47*, 4592–4594.
- (26) Leal-Egana, A.; Scheibel, T. *Biotechnol. Appl. Biochem.* **2010**, *55*, 155–167.
- (27) Yan, H.; Saiani, A.; Gough, J. E.; Miller, A. F. *Biomacromolecules* **2006**, *7*, 2776–2782.
- (28) Hu, X.; Lu, Q.; Sun, L.; Cebe, P.; Wang, X.; Zhang, X.; Kaplan, D. L. *Biomacromolecules* **2010**, *11*, 3178–3188.
- (29) Drury, J. L.; Mooney, D. J. *Biomaterials* **2003**, *24*, 4337–4351.
- (30) Vepari, C.; Kaplan, D. L. *Prog. Polym. Sci.* **2007**, *32*, 991–1007.
- (31) Kim, U. J.; Park, J. Y.; Li, C. M.; Jin, H. J.; Valluzzi, R.; Kaplan, D. L. *Biomacromolecules* **2004**, *5*, 786–792.
- (32) Matsumoto, A.; Chen, J.; Collette, A. L.; Kim, U. J.; Altman, G. H.; Cebe, P.; Kaplan, D. L. *J. Phys. Chem. B* **2006**, *110*, 21630–21638.
- (33) Wang, X.; Kluge, J. A.; Leisk, G. G.; Kaplan, D. L. *Biomaterials* **2008**, *29*, 1054–64.
- (34) Mackintosh, F. C.; Kas, J.; Janmey, P. A. *Phys. Rev. Lett.* **1995**, *75*, 4425–4428.
- (35) Parsegian, V. A.; Rand, R. P.; Fuller, N. L.; Rau, D. C. *Methods Enzymol.* **1986**, *127*, 400–16.
- (36) Fancy, D. A.; Kodadek, T. *Proc. Natl. Acad. Sci. U.S.A.* **1999**, *96*, 6020–4.
- (37) Hu, X.; Kaplan, D.; Cebe, P. *Macromolecules* **2006**, *39*, 6161–6170.
- (38) Urayama, K.; Takigawa, T.; Masuda, T. *Macromolecules* **1993**, *26*, 3092–3096.
- (39) Johnson, B. D.; Beebe, D. J.; Crone, W. C. *Mater. Sci. Eng.* **2004**, *24*, 575–581.
- (40) Murnaghan, F. D. *Am. J. Math.* **1937**, *59*, 235–260.
- (41) Slotta, U.; Hess, S.; Spiess, K.; Stromer, T.; Serpell, L.; Scheibel, T. *Macromol. Biosci.* **2007**, *7*, 183–188.
- (42) Papadopoulos, P.; Solter, J.; Kremer, F. *Eur. Phys. J. E* **2007**, *24*, 193–9.
- (43) Barth, A. *Prog. Biophys. Mol. Biol.* **2000**, *74*, 141–73.
- (44) Ma, L.; Gao, C.; Mao, Z.; Zhou, J.; Shen, J.; Hu, X.; Han, C. *Biomaterials* **2003**, *24*, 4833–41.
- (45) Martinez-Ruvalcaba, A.; Chornet, E.; Rodrigue, D. *Carbohydr. Polym.* **2007**, *67*, 586–595.
- (46) Scheibel, T.; Bloom, J.; Lindquist, S. L. *Proc. Natl. Acad. Sci. U.S.A.* **2004**, *101*, 2287–92.
- (47) Urry, D. W.; Pattanaik, A. *Ann. N.Y. Acad. Sci.* **1997**, *831*, 32–46.
- (48) Oh, S. H.; Park, I. K.; Kim, J. M.; Lee, J. H. *Biomaterials* **2007**, *28*, 1664–1671.